

Mitigation of Pulsed Interference to Redshifted HI and OH Observations between 960 and 1215 MHz²

J. R. Fisher

National Radio Astronomy Observatory¹, Green Bank, WV 24944
 rfisher@nrao.edu

Q. Zhang, Y. Zheng, S. G. Wilson

Electrical and Computer Engineering Dept., University of Virginia, Charlottesville, VA 22904
 qingzhang@virginia.edu, yz6n@virginia.edu, sgw@ee.virginia.edu
 and

R. F. Bradley

National Radio Astronomy Observatory¹, 2551 Ivy Rd, Charlottesville, VA 22903
 rbradley@nrao.edu

ABSTRACT

The neutral hydrogen 21-cm spectral line (1420.4 MHz) and the four 18-cm lines of the hydroxyl molecule (1612-1720 MHz) are observable at redshifts which put their measured line frequencies well below their protected frequency bands. Part of the redshift ranges ($z = 0.171$ - 0.477 for HI and $z = 0.37$ - 0.73 for OH) fall in the 960 to 1215 MHz band that is allocated to aircraft navigation. Most of the signals in this band are pulsed emissions of low duty cycle so much of the time between pulses is interference free. This paper outlines the structure and measured properties of signals in this band and demonstrates a signal processing strategy that is effective at removing the pulsed signals from spectra at sensitivities produced by several hours of integration.

Subject headings: instrumentation: miscellaneous — techniques: spectroscopic — radio lines: general

1. Introduction

Quasars emit strong continuum radiation at centimeter radio wavelengths. Since these objects are at cosmological distances their radiation must pass through clouds of neutral or partially ionized hydrogen in intergalactic space and in galaxies along the line of sight to the quasar. The hy-

drogen clouds selectively absorb radiation at the 21-cm (1420.4058 MHz) ground state transition, but the observed spectral line is Doppler shifted due to the recessional velocity of the absorbing cloud. The first high-redshift 21-cm absorption line was discovered by Brown & Roberts (1978) in the quasar 3C286 at 839.4 MHz ($z = 0.692$). Since then a considerable number of redshifted 21-cm neutral hydrogen (HI) absorption lines have been found (e.g., Briggs et al. 1989; Lane et al. 1998; Briggs 1999; Lane & Briggs 2001; Kanekar & Chengalur 2001a,b) to frequencies as low as 500 MHz and below in both blind searches of quasar spectra and at the redshifts of saturated Lyman- α

¹The National Radio Astronomy Observatory is a facility of the National Science Foundation operated under cooperative agreement by Associated Universities, Inc.

²A preliminary version of this work appeared in the NRAO Electronics Division Internal Report No. 313 which contains additional experimental detail.

absorption (see Rauch 1998).

Another spectral line emitter and absorber that can be detected at quite large redshifts is the hydroxyl molecule, OH. This molecule has four lines at 1612.231, 1665.402, 1667.359, and 1720.530 MHz, of which the two at 1665 and 1667 MHz are generally the strongest. Emissions from all of these lines can be very much enhanced by maser pumping from strong far-infrared radiation and stimulated emission caused by background continuum radiation along the line of sight (Baan, 1989). Galaxies in early stages of nuclear evolution provide both the far-infrared and continuum emission to produce extremely bright OH line emissions. Emitters of this sort are called OH megamasers because they are roughly a million times stronger than a typical source of OH radiation in our own Galaxy. The most distant reported megamaser has a redshift of $z = 0.2655$ (~ 1276 MHz) (Baan et al. 1992), and a growing number of detections have been reported out to a redshift of $z = 0.2$ (Baan et al. 1998; Darling & Giovanelli 2002a). Based on the observed line strengths, OH megamasers should be detectable at much greater redshifts (lower frequencies) (Darling & Giovanelli 2002b).

OH absorption can be seen in front of a strong continuum radio source, such as a quasar or radio galaxy, when there is insufficient far-infrared radiation near the OH gas cloud to pump maser emission. Like neutral hydrogen absorption, OH absorption may be seen at any redshift since the strength of the spectral line depends only on the flux density of the continuum source and the optical depth of the molecular gas. By studying the strengths of OH emissions and absorptions at a wide range of redshifts we can sample the physical conditions associated with infrared emission and OH cloud temperature and velocity structure throughout the history of the universe. These redshifted spectral lines are also important to the study of the evolution of the fine structure constant over the age of the universe (Darling 2003).

Redshifted HI and OH lines as well as the study of pulsars and other non-thermal physics in the universe make the radio spectrum below 1.5 GHz of considerable astrophysical importance. This paper describes the study of man-made radio signals in the part of this spectrum that is allocated to aircraft navigation (960-1215 MHz) and the demon-

stration of a technique for removing these signals from radio astronomical measurements. Transmissions from aircraft clearly dominate this frequency range. All of the measurements described were made at the National Radio Astronomy Observatory in Green Bank, WV, and the astronomical observations were taken with the 100-meter telescope (GBT). The signal processing algorithms applied to the data are described in a companion paper (Zhang et. al. 2005) referred to as Paper I.

2. Spectrum Use

Figure 1 shows a graphical depiction of spectrum use between 960 and 1215 MHz along with the corresponding redshift ranges for HI and the OH spectral lines near 1615 MHz. This frequency range is allocated to aircraft radio navigation, mainly used by civilian Distance Measuring Equipment (DME) and a compatible military Tactical Air Navigation (TACAN) system. The air-to-ground transmissions are confined to the 1025 to 1150 MHz range, and the 960-1024 and 1151-1215 Mhz bands are for the ground to air portion of this service. Sharing this band is the radar transponder system which uses 1030 MHz for ground-to-air interrogation and 1090 MHz for air-to-ground responses. Since many aircraft transmitting in the 1025-1150 MHz band are line-of-sight to Green Bank, this frequency range is quite full of strong signals during most of the day.

The DME system uses a time delay method for measuring the distance from an aircraft to a ground station. The aircraft begins determining its distance by transmitting short pulse pairs at a maximum rate of 150 pulse pairs per second on

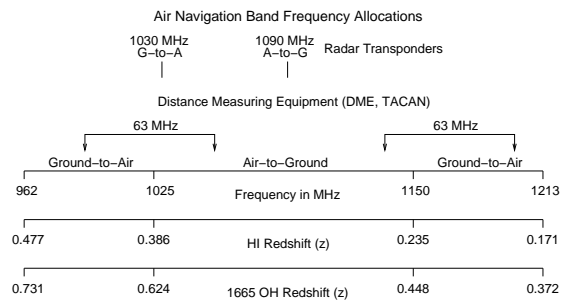


Fig. 1.— Frequency allocations in the aircraft radio navigation band between 960 and 1215 MHz.

the receive frequency of the selected ground station. After a fixed 50 microsecond delay from the received pulse time the ground station transmits a pulse pair back to the aircraft on a frequency either 63 MHz higher or lower than the aircraft transmission frequency. By measuring the delay between transmitted and received pulses, less 50 microseconds, the aircraft's DME unit can determine its distance from the ground station. This gives the slant-range distance rather than horizontal distance, but the latter can be computed from knowledge of the aircraft's altitude and the elevation of the ground station. Once the aircraft has established a steady dialog with the ground station it slows its pulse rate to a maximum of 30 pairs per second. Since up to 100 aircraft can simultaneously use the same ground station on the same frequency, the aircraft transmitters jitter their pulse transmission intervals to avoid locking onto ground station pulses intended for other aircraft. See Kline (1997)¹ and Forssell (1991) for more details.

TACAN uses the same pulse timing structure as DME, but it adds azimuth information to the ground-transmitted pulse powers. The civilian DME ground stations are generally co-located with VHF Omni-Range (VOR) stations, which provide the azimuth information. VOR operates in the 108 to 118 MHz band.

3. DME Signal Characteristics

DME transmission frequencies are 1 MHz apart. There are 126 aircraft transmission channels running from channel 1 at 1025 MHz through channel 126 at 1150 MHz. There are two transmission modes for each channel. In mode X the ground station transmission frequency is 63 MHz below the aircraft transmission frequency for channels 1-63 and 63 MHz above the aircraft frequency for channels 64-126. In mode Y the frequency spacing is reversed, i.e., the ground frequencies for channels 1-63 and 64-126 are 63 MHz above and below the aircraft frequencies, respectively. Hence, in mode Y the ground station transmissions are in the air-to-ground band. To avoid confusion between transmissions from aircraft and ground stations on the same frequency and to dis-

criminate pulses from random interference, pulses are always transmitted in pairs. From the aircraft in mode X the pulses are 12 microseconds apart, and in mode Y they are 36 microseconds apart. From the ground transmitter the pulses are 12 and 30 microseconds apart in modes X and Y, respectively. Mode X is used much more frequently than mode Y.

The transmitted pulses are approximately gaussian in shape as a function of time with a half-amplitude(voltage)-full-width of 3.5 microseconds.

$$V(t) \propto e^{-0.5(t/\sigma)^2} = e^{-2.7726(t/W)^2} \quad (1)$$

where t is time, and W is the full-width-half-maximum pulse width in the same units as t . Hence, from page 130 of Bracewell (1986) the individual pulse frequency spectrum will then be gaussian in shape

$$V(f) \propto e^{-0.5(\omega\sigma)^2} = e^{-3.5597(fW)^2} \quad (2)$$

where f is frequency in units of inverse W . The voltage spectrum full-width-half-maximum is then $0.8825/W$, or 0.252 MHz. The power spectrum full-width-half-maximum is $1/\sqrt{2}$ times that, or 0.178 MHz.

The peak pulse power from a transmitter on a large jet aircraft is 300 watts. Manufacturers of aircraft transceivers claim a useful range of about 550 km (300 nautical miles)², but aircraft altitude and the separations between ground stations on the same frequency will usually limit the range to less than 300 km. Smaller aircraft use peak powers on the order of 50 watts, which limits their ideal range to about 250 km. Smaller aircraft fly at lower altitudes and have a shorter line-of sight distance to the ground station. An aircraft at 1700 meters (5000 feet) altitude can expect a range of less than 100 km. Depending on the intended range of ground stations, the radii of their "standard service volumes"³ range from less than 25 to 130 nautical miles (46 to 240 km) (see Figures 6 and 7), although the airborne equipment is capable of longer useful ranges.

As described in Section 6, the peak power threshold for detecting a single pulse, with a mod-

¹<http://scholar.lib.vt.edu/theses/available/etd-112516142975720/unrestricted>

²<http://www.rockwellcollins.com/ecat/br/DME-4000.html?smenu=103>

³<http://www.flightsimaviation.com/index.php?p=aviationtheory&ch=6>

erate number of false detections, is about ten times the average noise power in a 0.25 MHz receiver bandpass centered on the pulse carrier frequency. This threshold corresponds to a power of 6.9×10^{-16} watts, or -151.6 dBW at the GBT receiver input with a noise temperature of 20 Kelvins. If we assume a transmitter power of 300 watts, a transmitting antenna gain of 0 dBi (decibels below isotropic gain), and a GBT sidelobe gain of -15 dBi, the maximum free-space distance at which a single pulse can be detected is about 2500 km. The detectable range of a 50-watt pulse is about 1000 km. Neglecting atmospheric refraction, the zero-degree horizon line-of-sight distance to an aircraft at 35,000 feet altitude is about 360 km so any aircraft DME transmitter whose line of sight to the GBT is above the horizon will generally be detectable in the GBT output with a signal filter matched to the pulse bandwidth. An aircraft with a 300-watt transmitter at 500 km distance would be detectable below the horizon if its diffraction loss is less than 14 dB.

As a comparison, the quoted receiver sensitivity of a representative DME ground station system⁴ is -117 dBW for 70% replies, and its minimum antenna gain is +8 dBi. If we again assume a 0 dBi transmitting antenna and 300 watts transmitted power, this corresponds to a useful line-of-sight range of 660 km. This is very close to the claimed useful range of a 300 watt aircraft transceiver.

4. Measured Pulse Properties

Figure 2 shows the composite spectrum seen by the GBT in the frequency range of 1085-1222 MHz at the low end of the tuning range of the 1.15-1.72 GHz, L-band receiver. It covers DME channels 65 through 126 and the frequencies of their corresponding mode X ground transmitters above 1150 MHz. Signals can be seen in every DME channel except below 1096 MHz where the radar transponder reply signals at 1090 MHz dominate the spectrum. A careful search for pulses from ground stations above 1150 MHz showed no detectable DME signals in these data. The top trace in Figure 12 shows an expanded portion of the spectrum between 1142 and 1152 MHz.

Figure 3 shows the waveform of a pair of strong

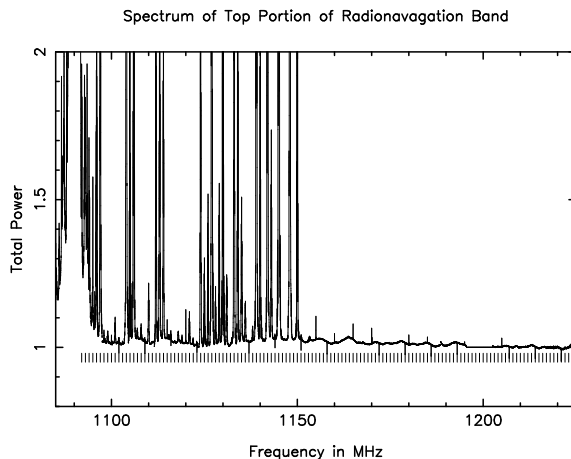


Fig. 2.— Composite spectrum measured on the GBT of the top half of the aircraft navigation band (DME Channels 65 to 126), February 20, 2004 between 12:00 and 14:00 EST. Each 7-Mhz spectrum segment is a 5-minute integration normalized to the receiver noise power. The segment near 1200 MHz was used as a reference spectrum so it is shown as a flat line. Hash marks below the spectrum show the DME 1-MHz channel frequencies. The vertical scale is fraction of system noise power.

⁴<http://www.amsjv.com/publications/ASI11181119SLqx.pdf>

pulses. These pulses nearly saturated the RF amplifiers so the negative peaks are slightly compressed. Plotted over the pulses are two gaussians with 3.5 microsecond full-width-half amplitude spaced 12 microseconds apart. This particular transmitter appears to truncate its pulses somewhat faster than a gaussian curve, hence the spectral bandwidth will be somewhat wider than the values stated in Section 3. Also, the pulses are a couple of tenths of a microsecond closer together than 12 microseconds. This may be typical of the tolerances to be expected.

Figure 4 shows the Fourier transformed amplitude (voltage) spectrum of the pulses shown in Figure 3. As expected from the measured pulse shape, the amplitude spectrum is wider than would be expected from a gaussian pulse shape of 3.5 microseconds half-amplitude width. Also, the carrier frequency is about 21 kHz lower than the nominal 1142.0 MHz of this transmitter channel. (A manufacturer's DME transceiver brochure⁵ states a frequency stability specification of ± 100 kHz.) The 83 kHz modulation period in this spectrum is due to coherent beating of the two pulses. In Paper I the use of matched filters for optimum pulse detection is explained, and the frequency offset observed here shows that the filter must match single pulses rather than pulse pairs to avoid missing pulses that fall in the nulls of a two-pulse matched filter.

Figure 5 shows a fairly typical train of pulses from several aircraft. There appear to be at least five transmitting aircraft in this plot as surmised from the tracks of pulse power as a function of time. Three of the transmissions began in the time interval shown at about 52.5, 53.0, and 57.5 seconds. Each began with a repetition rate of about 20 pulses per second and then slowed to about 4 or 5 pps. This is a considerably slower pulse rate than the 120-150 and 24-30 pps acquisition and post-acquisition rates described in the literature (Forsell 1991). One manufacturer's product brochure⁶ states that it is capable of scanning three DME channels at 12.5 milliseconds per channel so that the DME samples each channel 27 times each second. Even when covering three channels at once,

⁵<http://www.rockwellcollins.com/ecat/br/DME-42.442.html?smenu=103>

⁶<http://www.rockwellcollins.com/ecat/br/DME-42.442.html?smenu=103>

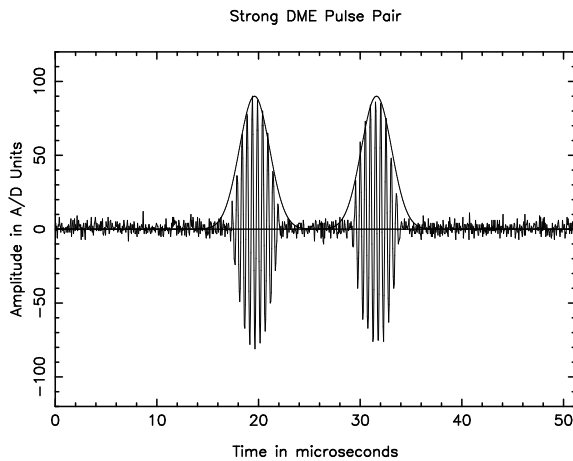


Fig. 3.— Strong pulse pair measured at 1142 MHz. The waveform is slightly saturated on negative peaks. The gaussian curves are 3.5 microseconds half-amplitude width and 12 microseconds apart.

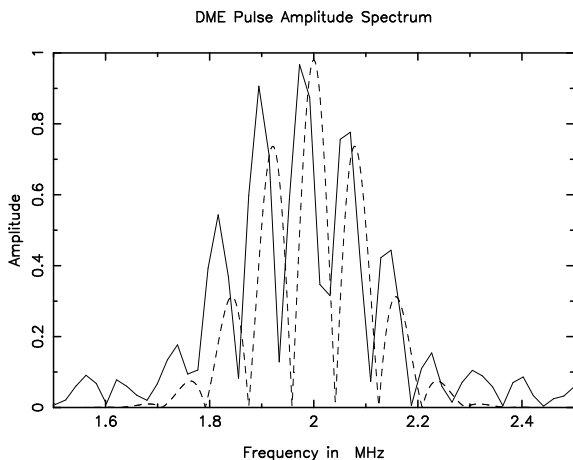


Fig. 4.— Amplitude spectrum of the pulse pair in Figure 3. The dashed curve is the spectrum expected from a pair of gaussian pulses of 3.5 microseconds amplitude width and 12 microseconds apart with a carrier frequency of 1142.000 MHz.

it can lock-on in less than one second. This fits the observed behavior of the three pulse tracks in Figure 5. After acquisition the transceiver appears to scan the channels at a slower rate, which is advantageous from radio astronomy’s point of view since the average power received from each aircraft transmitter is lower at a given frequency.

The detection threshold used in generating Figure 5 is about ten times the average receiver noise power in the 0.25 MHz bandwidth of the pulse. In Section 3 we calculated this threshold to be -151.6 dBW at the GBT receiver input with a noise temperature of 20 Kelvins. The stated receiver sensitivity of a commercial DME ground station is -117 dBW⁷. If we assume that the system noise temperature of the DME station is 400 K, then the GBT detection threshold used is about 21.6 dB = $151.6 - 117 - 10 * \text{Log}_{10}(400/20)$ lower in terms of system noise power than is used in the DME station receiver. The DME ground station detection threshold would correspond to a level of about 1.8 on the vertical scale of Figure 5. We surmise that this threshold difference is roughly the signal processing margin used in the DME station receiver to avoid false detections or detections of distant aircraft interrogating other stations on the same frequency.

5. Ground Station Locations

Figure 6 shows the location of DME stations in the eastern U. S. that are found in the aeronautical information data base.⁸ Stations with different service radii and altitude ranges are shown with different symbols.

An example of the locations of stations operating in a specific DME channel is shown in Figure 7. The large circles illustrate the greater range of the high-altitude stations. Around the location of Green Bank two irregular contours show the line-of-sight distance to an aircraft just above the horizon as seen from the prime focal point of the GBT for aircraft altitudes of 15,000 and 35,000 feet above sea level. The horizon contours do not take atmospheric refraction into account, but refraction extends the effective line-of-sight range by only 5 to 10%.

⁷<http://www.amsjv.com/publications/ASI11181119SLq.pdf>

⁸<http://www.naco.faa.gov/index.asp?xml=naco/catalog/charts/digital/daicd>

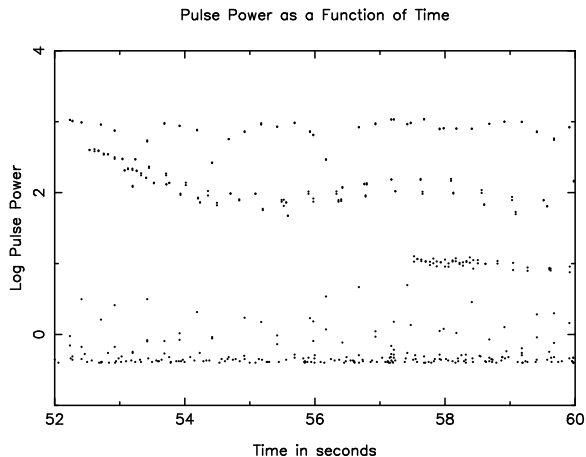


Fig. 5.— Measured powers of individual pulses vs time at 1145 MHz (DME Channel 121) recorded 5:53 EST on January 27, 2004 with the GBT L-band receiver. Individual pulses in each pulse pair are shown.

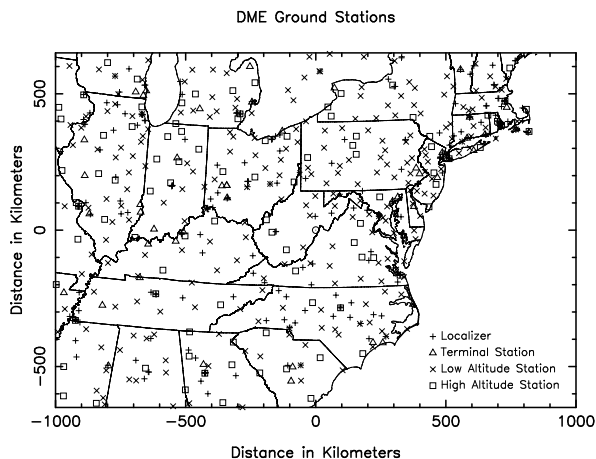


Fig. 6.— The locations of all DME stations around Green Bank found in the Navaid Digital Data File of the Digital Aeronautical Information CD data base from the National Aeronautical Charting Office of the Federal Aviation Administration. The high altitude stations are marked with squares, the low altitude stations are marked with X’s, the terminal stations are marked with triangles, and localizer stations are marked with +’s. The location of Green Bank is marked with a circled dot at the coordinates (0,0).

6. Pulse Detection and Statistics

To generate a test data set under conditions close to typical GBT observing a series of on-off scans were taken on the radio source 0952+176 which has a continuum flux density of about 1.4 Janskys and a narrow HI absorption line at 1147.5 MHz with a depth of about 15 mJy (Kanekar & Chengalur 2001b). These observations used 8-bit baseband sampling of a 10 MHz bandwidth centered on 1147 MHz. This passband included DME channels 119 (1141 MHz) through 126 (1150 MHz) plus channel 118 at the lower edge of the band and a bit of spectrum above the air-to-ground frequency range. Two observing sessions were recorded: January 27, 2004 from 05:24 to 07:37 EST (13:29 to 15:42 LST) and February 23, 2004 from 17:32 to 20:01 EST (03:35 to 05:54 LST). Unless otherwise noted, all of the pulse property measurements used the January data. The February session was used to verify the efficacy of pulse blanking described in Section 9

These data were processed in one-minute chunks, which was the file size into which the data acquisition computer divided the 8-bit samples. The A/D input level was such that the noise voltage rms value spanned about four A/D levels. The sample interval was 50 nanoseconds (20 mega-samples per second).

The first major signal processing step was to scan every one-minute data file for pulses and create a list of pulse times and powers for each DME channel in the spectrum. The pulse detection scheme is described in detail in Paper I. The basic process was to Fourier transform one-megasample (50 millisecond) data lengths into the frequency domain, apply a matched filter to each DME frequency, transform back to the time domain, square to get power, and search this power sample series for peaks above a chosen threshold. The threshold was set to 15 times the median power value in the first 50-millisecond sample of each DME channel. This was roughly 10 times the average power level in a channel filter passband between pulses and produced a modest number of false detections on random noise. Pulse peaks were then found starting with the strongest one. Data in a 15-microsecond window centered on the found peak were set to zero so that this pulse and surrounding data would not be detected in the remainder

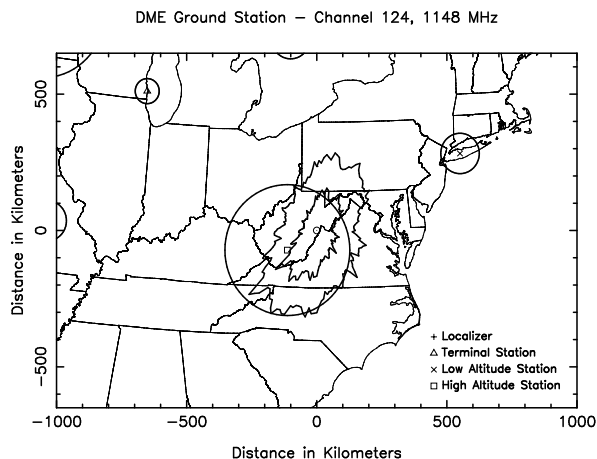


Fig. 7.— The locations of DME channel 124 (1148 MHz) stations. The range of each station is shown by the circle centered on it: 240 km for high altitude stations, 74 km for low altitude, and 46 km for terminal stations. No localizer stations are shown for this channel, but they would be surrounded by 20 km radius circles. The irregular contours around Green Bank, WV (indicated by the circled dot) show the line-of-sight horizons of the GBT prime focus point for aircraft at altitudes of 4.6 (inner) and 10.7 (outer) km (15,000 and 35,000 feet).

of the peak search. This window was small enough to allow the second pulse in a 12-microsecond pair to be detected but wide enough to suppress most of the wings of strong pulses. The final pulse list was sorted by pulse time for further analysis and for use in blanking pulses in the original data set.

During the analysis of pulse statistics the strongest pulses were found to affect the entire 10-MHz spectrum causing false detections in channels other than the one containing the transmitted pulse. To remove this spurious effect from the analysis the sorted pulse lists were searched for strong pulses, and all pulses in other channels within five microseconds of each strong pulse were deleted from the list.

The filter applied to each DME channel frequency was chosen by visually matching the envelope of the spectrum shown in Figure 4 to a gaussian function. This function had a full-width-half-maximum width of 0.25 MHz in the voltage domain. This corresponds to a power noise equivalent width of 0.188 MHz. If a DME pulse transmitter were as much a 0.1 MHz off in frequency, as is permitted in at least one manufacturer's specs, the filter response would be down by about 4 dB, but most of the pulses appeared to be within about 30 kHz of the nominal channel frequencies.

We expect pulses to arrive in pairs, either 12 or 36 microseconds apart for mode X or Y, respectively. This should be evident in a histogram of adjacent pulse separations. Figure 8 shows four such histograms for one minute of measurements of four different DME channels. All four channels show a clear peak at 12 microseconds, and channel 126 shows a small number of mode Y pulses at 36 microseconds. The nearest ground station assigned to channel 124 is in Beckley, WV so there is a lot of activity on this channel. The large number of pulses on channel 124 at spacings other than 12 microseconds may be due to echoes of strong pulses from terrain around Green Bank as described in Section 8.

Figure 9 shows examples of pulse power distributions, ranging from the detection threshold to the pulse saturation limit of the GBT receiver for four DME channels in one five-minute scan. The solid and dashed lines in these plots show the difference between, respectively, all detected pulses and only those pulses that have detected neighbors near 12 microseconds away. The difference

gives an upper limit on the number of false detections due to random noise or sources of non-DME pulses. An interesting feature of these plots is that the number of known pulse pairs per logarithmic power interval does not appear to be rising steeply with decreasing power near the detection limit. This is fairly typical of most of the data in these two hours of GBT observations.

Two important questions to ask are how much power remains in pulses below the detection threshold, and is this sufficient to be noticeable in the spectrum with detected pulses removed? To answer these questions an assumption is needed for the number distribution of the undetected pulses as a function of power. Assuming a power law for the pulse power distribution

$$\log\left(\frac{n(I)}{n_o}\right) = \alpha \log\left(\frac{I}{I_o}\right) \quad (3)$$

or

$$\frac{n(I)}{n_o} = \left(\frac{I}{I_o}\right)^\alpha \quad (4)$$

then the total power in the undetected pulses will be

$$p = \sum_i n(I_i) I_i = \sum_i n_o \left(\frac{I_i}{I_o}\right)^\alpha I_i \quad (5)$$

If we do the summation using logarithmic intervals in I_i of 0.1 for various values of α we get the values of p/I_o shown in the second column of Table 1. For example, for $\alpha = 0$, if I_o is the pulse power detection threshold and $n_o = 1$, the cumulative power from all pulses below the threshold will be 4.9 times the power in one pulse at the threshold level. For values of $\alpha \leq -1$ the summation in Equation 5 will diverge at low powers, and such a distribution will give infinite power without a low power cutoff. Since each DME channel will be occupied by a finite number of aircraft transmissions such a divergence is not possible in practice.

To determine limits on the number of pulses under the detection threshold that can be tolerated in an astronomical spectrum, assume a five-minute integration with a spectral resolution of 20 kHz (5.2 km/s at 1.15 GHz). The rms noise power in each spectral channel will be $4.1 \times 10^{-4} = 1/(300^s \times 2 \times 10^4 \text{ Hz})$ times the total noise power in the channel. Most pulses stronger than 15 times the average noise power in the bandwidth of the pulse will be detected. The width of one

pulse is 3.5 microseconds so the power in one pulse averaged over the 300 second integration is $15 \times 3.5 \times 10^{-6}/300 = 1.75 \times 10^{-7}$ times the noise power in the pulse bandwidth. Hence, there could be $4.1 \times 10^{-4}/1.75 \times 10^{-7} = 2343$ pulses at the detection threshold (7.8 per second) without significantly affecting the spectrum. If the undetected pulse powers were distributed with a power law of $\alpha = -0.5$, then there could be $2343/9.2 = 255$ pulses (0.85 per second) in the interval just below the detection thresholds and more at weaker powers according to the power law. The tolerable number of pulses per second in the interval just below the detection threshold for various values of α is given in the third column of Table 1, and the total pulse number limits are plotted in Figure 9.

The limits shown on the left side of the plots in Figure 9 show that the unblanked pulses are close to being detectable in the astronomical spectra for the more active DME channels measured. The assumptions that went into the calculation of these limits may be a bit pessimistic. In an on-off observing procedure the average pulse power will tend to cancel, and the one-sigma power limit is probably a bit too stringent. Nevertheless, the unblanked pulses are of some concern, and improvements in pulse detection sensitivity may be worth pursuing. For a given pulse power distribution, the number of tolerable pulses below the detection threshold is inversely proportional to the threshold power.

7. Signal Power vs DME Station Distance

One might expect to measure lower average signal powers on DME channels where the nearest

Table 1: Undetected pulse residual power and limits on the number of pulses per second in the interval just below the detection threshold in a 300-second integration for different pulse power distributions

α	p/I_o	$N(I_o)/second$
+inf	1.0	7.8
0	4.9	1.6
-0.25	6.3	1.2
-0.50	9.2	0.85
-0.75	17.9	0.43

ground station is farther away. To test this assumption the relative average powers of all pulses detected were plotted as a function of nearest station distance. The results are shown in Figure 10 for all channels shown in Figure 2 above 1100 MHz.

A notable feature of Figure 10 is that relatively strong signals can be seen for stations out to at least 500 kilometers distance, particularly for high-altitude stations. There may be saturation effects in the power of signals from nearby stations so the upper envelope of the distribution may be somewhat suppressed at short distances. As expected, the signals associated with low-altitude stations are generally weaker than those associated with high-altitude stations. Not all signals come from aircraft that are interrogating the nearest station so conclusions can be drawn only from trends in this figure and not from individual data points. There was a slight tendency for the total pulse power to increase with time over the observing session as one might expect in the early morning hours as aircraft begin their flight schedules.

8. Echoes

The broad distribution of pulse spacings shown in the top right panel of Figure 8 could be due to echoes of strong pulses from surrounding terrain as were measured in pulses from a ground-based air surveillance radar⁹. To test this hypothesis average pulse power profiles were computed in a number of one-minute intervals for the strongest pulses that did not saturate the receiver system. The results for the DME channel in the top right panel of Figure 8 are shown in Figure 11. All of the profiles show strong evidence of echoes out to a delay of about 70 microseconds. This agrees well with the measured distribution of radar pulse echo delays. Echo pulse powers relative to the direct pulse powers range from about -20 dB at small delays to less than -40 dB, which is the detection limit of these measurements. The solid trace in Figure 11 shows what could be an isolated single reflection at a delay of about 45 microseconds.

⁹<http://www.gb.nrao.edu/~rfisher/Radar/analysis.html>

9. Pulse Blanking in the Integrated Spectra

To remove DME signals from the data the list of detected pulse times in each one minute record were used to set blanking windows in the raw sampled data. Each blanking window was 12 microseconds wide, and it was applied to each detected pulse, including a small fraction of false detections due to random noise. Unlike the strategy described in Paper I, a detected pulse in any of eight DME channels (1143-1150 MHz) resulted in blanking data for the full 10 MHz bandwidth. In the January 27 data this resulted in a blanked data fraction ranging from 0.5 to 1.1% of the data samples with the fraction increasing with time over the 05:24 to 07:37 EST observing period. A smaller fraction of data could be blanked if one-megahertz sections were processed separately, blanking only on pulses from one DME channel at a time. However, this adds the complication of stitching the spectra back together seamlessly, and strong pulses from adjacent channels that splatter across the spectrum may not be blanked as effectively. Even in the busiest part of the day the data lost probably will not be greater than about 2% with full 10-MHz spectrum blanking. Simultaneous processing of wider bandwidths would lose proportionately greater fractions of data.

One consequence of blanking small windows of sampled data is that power is lost, and extra sidelobes will be generated on narrowband signals. The fraction of power lost and the total power in the sidelobes will be equal to the blanking fraction. One or two percent loss usually will not affect the astronomical data significantly, but this effect needs to be kept in mind. In principle, one can compute and correct for the sidelobe pattern and power loss from the known blanking pattern, if the extra computational load is warranted.

Figure 12 shows the total power spectrum of one minute of data. Strong DME signals can be seen in the top spectrum, without blanking, in four of the channels, and weak signals can be seen in at least three other channels, not including 1142 MHz. The middle trace shows the spectrum from the same data with pulse blanking. To the noise level of this spectrum, all of the blanked DME signals have been suppressed. There are still a few RFI signals in the spectrum, but most of these are

quite narrow and can be excised by deleting one to three spectral channels around each narrow spike as shown in the bottom spectrum. None of the narrow spikes are likely to be associated with the DME signals.

To test how well pulse blanking works on long astronomical integrations the data from the January 27 and February 23 two-hour observing sessions of the quasar 0952+176 were run through the blanking algorithms. The observing sequence was alternately 5 minutes on source and 5 minutes off. The total on- plus off-source integration times in the sessions were 108 and 140 minutes, respectively. The data were summed with weighting of each spectrum by the inverse of the square of the estimated system temperature for each ten-minute on-off scan pair. The weighted system temperature estimates in each session were 21.8 and 23.4 Kelvins, respectively. The February session was observed at lower elevation angles.

Figure 13 shows the integrated spectra from the first observing sessions with and without pulse blanking and narrowband spike removal. A similar plot for the second session looks much the same. The weak absorption feature at 1147.5 MHz can be seen in the blanked spectra. There is a hint of residual DME signal in the strongest channel frequencies as we expect from the analysis in Section 6, but this does not affect the detection of relatively narrow spectral features significantly.

Figures 14 and 15 show the integrated spectra from both observing sessions. The expected 52 kHz differential Doppler shift in the HI line frequency between the two observing sessions can be seen in these plots. The February 23 spectrum is shifted to the January 27 Doppler offset before taking the weighted average of the two spectra. The vertical scale in Figure 15 is shown approximately in Janskys. The continuum level around 0.97 Jy is less than the published 1.4 Jy, but the measured peak line depth to continuum ratio of 0.0127 ± 0.02 is quite close to the published value of 0.013 by Kanekar & Chengalur (2001b). The same paper shows a line half-power width of about 35 kHz, which is consistent with the line widths shown in Figure 15.

The measured single-channel rms noise values of the three spectra shown in Figure 15, without any baseline removal, are 3.7, 3.2, and 2.8 milli-Janskys, respectively, bottom to top. From the

resolution bandwidth and integration times and the known correlation loss due to the way the spectra are generated in the FFT algorithm the expected rms values are 3.6, 3.2, and 2.4 millijanskys, respectively. Hence, the pulse blanking scheme described in this paper is fully effective with minimal loss of data and little, if any, loss in sensitivity.

10. Computational Requirements and Future Work

All of the signal processing described in this report was done on a general purpose processor. Implementation of faster algorithms remains to be done, but it is clear from a rough analysis of the computational load that finding DME pulses in the data and computing blanked spectra for more than a few megahertz of bandwidth will require a fairly large computer cluster or one of the parallel processing digital technologies. We are investigating the feasibility of programming the critical algorithms into field programmable gate arrays (FPGAs). Much of the science to be accomplished with the technique described in this paper and Paper I will require real-time processing of more than 100 MHz of bandwidth.

More sensitive pulse detection will help remove weaker pulses that are probably leaking into the pulse-blanked spectra shown in this paper. The filter used for pulse detection is reasonably close to optimum so the only route for weaker pulse detection is an antenna and RF amplifier system that has a higher signal-to-noise ratio on DME signals. The GBT has an approximate average sidelobe gain of -15 dBi and a system temperature of 20 Kelvins. If a separate antenna with a gain of +6 dBi and a pre-amplifier that produces a system temperature of 400 Kelvin were used to receive the DME signals, then one could realize an increase in SNR of about $8 \text{ dB} = 6 \text{ dBi} - (-15 \text{ dBi}) + 10 \log(20\text{K}/400\text{K})$. Implementation of a receiving system for this purpose is now underway.

Facilities: NRAO(GBT).

REFERENCES

Baan, W. A., Rhoads, J., Fisher, K., Altschuler, & D. R., Haschick, A. 1992, ApJ, 396, L99

- Baan, W. A., Salzer, J. J., & LeWinter, R. D. 1998, ApJ, 509, 633
- Bracewell, R. N. 1986, *The Fourier Transform and Its Applications*, (2d ed., revised; New York: McGraw-Hill)
- Briggs, F.H., Wolfe, A. M., Liszt, H. S., Davis, M. M., & Turner, K. L. 1989, ApJ, 341, 650
- Briggs, F. H. 1999, in ASP Conf. Ser. 156, *Highly Redshifted Radio Lines*, ed. C. L. Carilli et. al. (San Francisco: ASP), 16
- Brown, R. L. & Roberts, M. S. 1978, ApJ, 184, L7
- Darling, J. 2003, Phys. Rev. Lett., 91, 011301
- Darling, J., & Giovanelli, R. 2002, AJ, 124, 100
- Darling, J., & Giovanelli, R. 2002, ApJ, 572, 810
- Forssell, B. 1991, *Radionavigation Systems*, (New York: Prentice Hall)
- Kanekar, N., & Chengalur, J. N. 2001a, MNRAS, 326, 631
- Kanekar, N., & Chengalur, J. N. 2001b, A&A, 369, 42
- Kline, P. A. 1997, Ph.D. Thesis, Virginia Polytechnic Institute and State University
- Lane, W., Smette, A., Briggs, F., Rao, S., Turnshek, D., & Meylan, G. 1998, AJ, 116, 26
- Lane, W. M., & Briggs, F. H. 2001, ApJ, 561, 27
- Rauch, M., 1998, ARA&A, 36, 267
- Zhang, Q., Zheng, Y., Wilson, S. G., Fisher, J. R., Bradley, R. F. 2004, AJ, 000, 0000 (companion paper submitted for publication together, "Excision of DME Interference from Radio Astronomy Signals") (Paper 1)

This 2-column preprint was prepared with the AAS L^AT_EX macros v5.2.

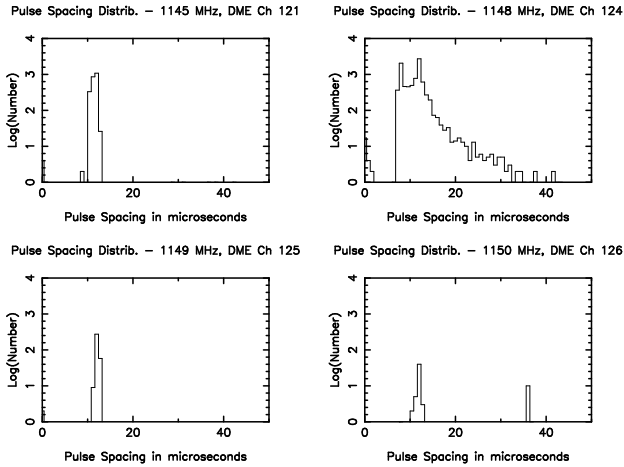


Fig. 8.— Distribution of adjacent pulse spacings for four DME channels measured for one minute near 06:22 EST of January 27. The continuous distribution of pulse spacings shown in the top right panel is probably due to echoes from surrounding terrain as explained in the text associated with Figure 11

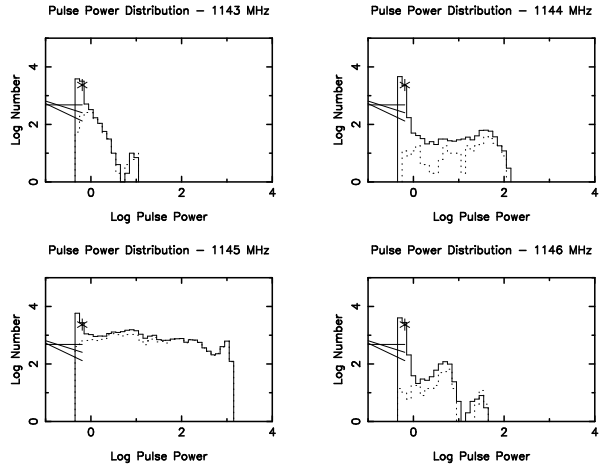


Fig. 9.— Number distribution of detected pulses as a function of relative pulse power for DME channels 119-122 in a five minute scan recorded at 06:22 EST of January 27. The solid lines show all detected pulses, and the dashed lines show only pulses that are paired with another between 11 and 13 microseconds away. On the left side of each plot are plotted the pulse number distribution limits to remain undetected in a five-minute integration as described in the text. The star marks the limit if all unblanked pulses are at the detection threshold ($\text{Log}_{10}(\text{power}) \approx -0.2$). The horizontal straight line is for a number density index of $\alpha = 0$, and the sloped lines are for $\alpha = -0.5$ and -0.75 . Pulses saturate the receiver at $\text{Log}_{10}(\text{power}) \approx 3.0$.

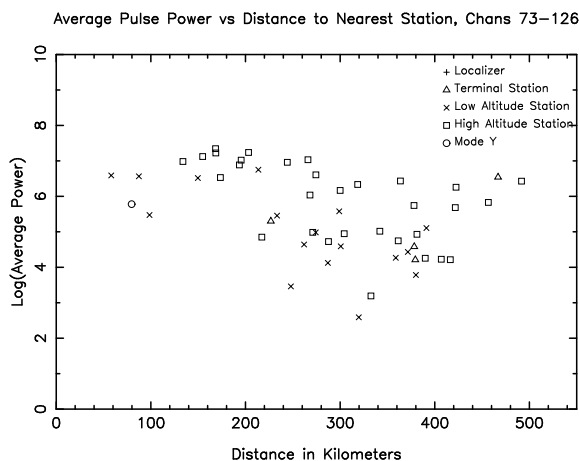


Fig. 10.— Relative average signal power in five minutes as a function of the distance to the nearest DME station from Green Bank for all DME channels above 1100 MHz shown in Figure 2. The high, low, terminal and localizer station symbols are the same as in Figures 6 and 7.

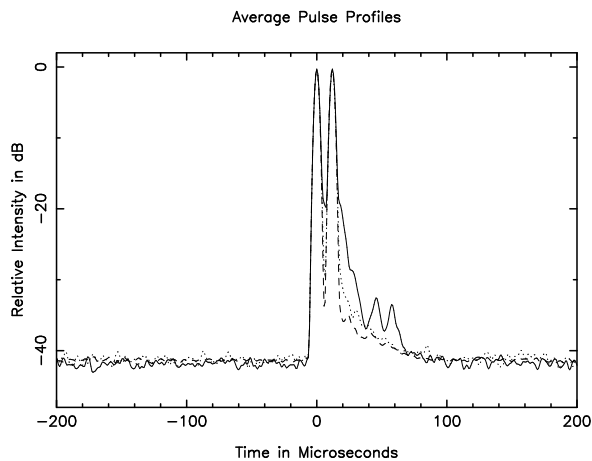


Fig. 11.— Average pulse profiles at 1145 MHz (DME channel 121, cf. the top right panel in Figure 8) in one minute scans recorded at 05:24 (solid), 07:06 (dashed), and 07:27 (dotted) EST. Only isolated pulses in a 2-dB range of amplitudes just below GBT receiver saturation were included in the averages.

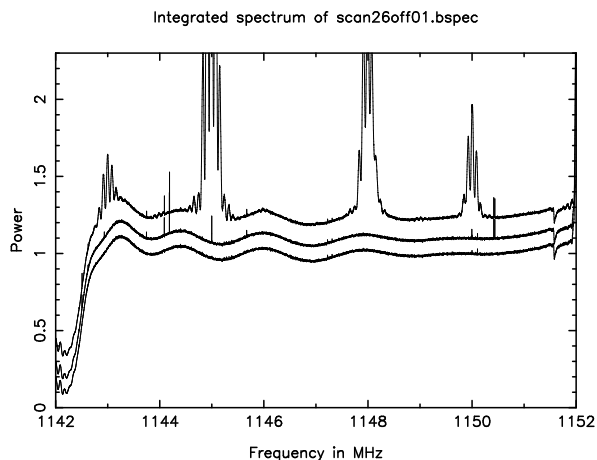


Fig. 12.— Total power spectra computed for one minute of data recorded at 07:23 EST on January 27 on the GBT. The spectra contain 8192 channels (1.2 kHz channel spacing). The top trace is without blanking. The middle trace is with blanking, and the bottom trace is with blanking and narrowband signal removal.

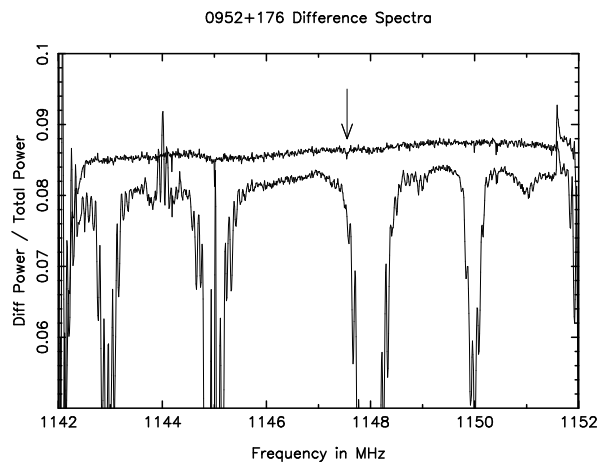


Fig. 13.— Averaged (ON - OFF) / OFF spectra for all of the January 27 data. The vertical scale is in fraction of the system noise power. The bottom spectrum is without blanking and the top spectrum is with blanking and narrowband spike removal. The arrow marks the frequency of the absorption line in 0952+176.

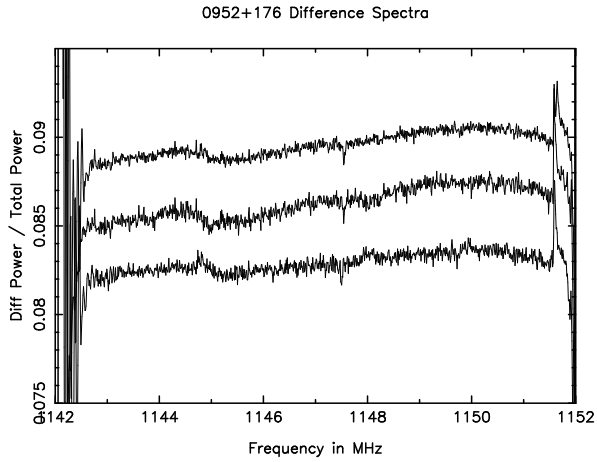


Fig. 14.— Averaged $(\text{ON} - \text{OFF}) / \text{OFF}$ spectra for all of the data with blanking and narrowband spike removal. The middle spectrum is from January 27; the bottom spectrum is from February 23; and the top spectrum is the average of all data with the February 23 spectrum shifted by the expected differential Doppler shift. The spectra are offset vertically by a small amount for clarity.

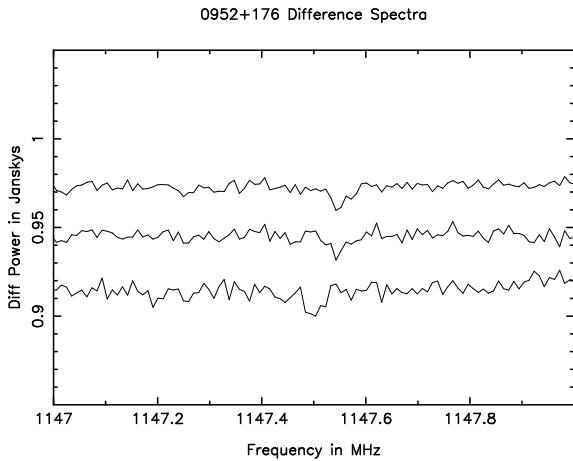


Fig. 15.— Same as Figure 14 but expanded around the 1147.5 MHz HI absorption feature and with the vertical scale in Janskys. The lower two spectra are offset vertically by a small amount for clarity.